



**HAL**  
open science

## Effects of static magnetic field on the sulfate metabolic pathway involved in *Magnetospirillum magneticum* AMB-1 cell growth and magnetosome formation

Haitao Chen, Hongkai Shi, Changyou Chen, Yangkun Jiao, Pingping Wang, Chuanfang Chen, Jinhua Li, Long-Fei Wu, Tao Song

### ► To cite this version:

Haitao Chen, Hongkai Shi, Changyou Chen, Yangkun Jiao, Pingping Wang, et al.. Effects of static magnetic field on the sulfate metabolic pathway involved in *Magnetospirillum magneticum* AMB-1 cell growth and magnetosome formation. *Journal of Applied Microbiology*, 2023, 134 (12), 10.1093/jam-bio/lxad302 . hal-04398404

**HAL Id: hal-04398404**

**<https://amu.hal.science/hal-04398404>**

Submitted on 31 Jan 2024

**HAL** is a multi-disciplinary open access archive for the deposit and dissemination of scientific research documents, whether they are published or not. The documents may come from teaching and research institutions in France or abroad, or from public or private research centers.

L'archive ouverte pluridisciplinaire **HAL**, est destinée au dépôt et à la diffusion de documents scientifiques de niveau recherche, publiés ou non, émanant des établissements d'enseignement et de recherche français ou étrangers, des laboratoires publics ou privés.



21 **ABSTRACT**

22 **Aims**

23 Magnetotactic bacteria (MTB) can use their unique intracellular magnetosome organelles to swim  
24 along the Earth's magnetic field. They play important roles in the biogeochemical cycles of iron and  
25 sulfur. Previous studies have shown that the applied magnetic fields could affect the magnetosome  
26 formation and antioxidant defense systems in MTB. However, the molecular mechanisms by which  
27 magnetic fields affect MTB cells remain unclear. We aim to better understand the interactions between  
28 magnetic fields and cells, and the mechanism of MTB adaptation to magnetic field at molecular levels.

29 **Methods and results**

30 We performed microbiological, transcriptomic and genetic experiments to analyze the effects of a weak  
31 static magnetic field (SMF) exposure on the cell growth and magnetosome formation in MTB strain  
32 *Magnetospirillum magneticum* AMB-1. The results showed that a 1.5 mT SMF significantly promoted  
33 the cell growth but reduced magnetosome formation in AMB-1, compared to the geomagnetic field.  
34 Transcriptomic analysis revealed decreased expressions of genes primarily involved in the sulfate  
35 reduction pathway. Consistently, knockout mutant lacking adenylyl-sulfate kinase CysC did no more  
36 react to the SMF and the differences in growth and Cmag were disappeared. Together with  
37 experimental findings of increased reactive oxidative species in the SMF-treated WT strain, we  
38 proposed that *cysC*, as a key gene, can participate in the cells growth and mineralization in AMB-1 by  
39 SMF regulation.

40 **Conclusions**

41 This study suggests that the magnetic field exposure can trigger a bacterial oxidative stress response  
42 involved in AMB-1 growth and magnetosome mineralization by regulating sulfur metabolism pathway.  
43 CysC may serve as a pivotal enzyme in mediating sulfur metabolism to synchronize the impact of SMF  
44 on both growth and magnetization of AMB-1.

45

46 **Keywords:** static magnetic field, magnetosomes, transcriptomic analysis, sulfur metabolism, reactive  
47 oxidative species.

48 **Impact Statement**

49 These findings provide new insights into the biological adaptation mechanisms involved in magnetic  
50 field and further improve the current knowledge of biomineralization and biogeochemical cycles in  
51 prokaryotic systems.

52 **Introduction**

53 Geomagnetic field (GMF) acts as a signal to help various microorganisms adapt to environmental  
54 changes and/or as energy to randomly affect biochemical reactions and metabolic pathways as well as  
55 microorganism-specific processes such as carbon respiration, sulfate reduction, sulfur oxidation,  
56 denitrification, nitrogen fixation, and iron reduction (Li et al., 2022b; Madsen, 2011; Sanyal et al.,  
57 2019). Magnetotactic bacteria (MTB) might represent one of the earliest microorganisms on Earth that  
58 have been found to be particularly sensitive to GMF (Lin et al., 2018). They are able to orient and  
59 migrate along GMF line, which is known as “magnetotaxis”. This behavior makes MTB adapt to their  
60 physiological functions and environmental change, and play important roles in the biogeochemical  
61 cycles of iron and sulfur (Frankel et al., 1981; Komelli, 2007; Li et al., 2022b; Schüler, 2002). In fact,  
62 magnetotaxis has been shown to be beneficial to the growth of MTB and becomes essential at low cell  
63 densities (Zhang et al., 2014). Furthermore, MTB have demonstrated potential for biomedical  
64 applications such as targeting and delivering into deep tumor tissues due to their capability of  
65 navigating using external magnetic fields (Jadhav and Prabhu, 2022; Taherkhani et al., 2014; Wang et  
66 al., 2022).

67

68 MTB can synthesize intracellular membrane-enclosed, nanosized, and chain-arranged magnetite and/or  
69 greigite crystals called magnetosomes (Rajalakshmi et al., 2022; Spring and Bazylinski, 2002). They  
70 use magnetosomes for orientation, which provides both a simple biophysical mechanism for  
71 magnetoreception and an unambiguous example of an Earth-strength magnetic effect on biology  
72 (Bazylinski and Frankel, 2004; Kolinko et al., 2014; Philippe and Wu, 2010; Schüler, 2007). In the last  
73 decade, the detailed mechanism of magnetosome formation has been gradually elucidated (Murat et al.,  
74 2012; Raschdorf et al., 2016; Uebe and Schüler, 2016; Wan et al., 2022). In addition to forming  
75 magnetosomes, other intracellular inclusion body types, such as sulfur globules, polyphosphates,  
76 polyhydroxybutyrate, calcium carbonate, silica, and ferrosomes, are observed in some MTB,  
77 suggesting that they have diverse metabolic mechanisms to adapt to the environment (Chen et al., 2015;  
78 Cox et al., 2002; Grant et al., 2022; Li et al., 2022c; Li et al., 2021a; Liu et al., 2021).

79

80 Previous studies have found that MTB can efficiently eliminate intracellular reactive oxygen species  
81 (ROS) through their magnetosome crystals and proteins, which are believed to play an important role

82 in life processes (Chen et al., 2020a; Chen et al., 2020b; Guo et al., 2012; Li et al., 2017; Lin et al.,  
83 2020). Some MTB might have adapted to couple redox-related metabolic activity and magnetosome  
84 biomineralization to result in consequent cell magnetotaxis through GMF-guided upward sulfur  
85 shuttles and downward nitrate shuttles (Li et al., 2021a). It has been demonstrated that the nitrate and  
86 nitrite reductases of the denitrification pathway have the additional key functions by participating in  
87 redox reactions required for magnetite biomineralization in *Magnetospirillum. magneticum* AMB-1 and  
88 *Magnetospirillum gryphiswaldense* MSR-1 (Li et al., 2012; Wang et al., 2011). These results suggest  
89 that redox-related metabolic activities and magnetosome biomineralization are vital factors in the  
90 adaptation of MTB to the biomagnetic environment. Moreover, studies by Frankel et al., (1981) and  
91 Zhang et al., (2010) have demonstrated that the redox gradient configuration in combination with the  
92 magnetic field direction are determining factors that select the magnetotactic polarity of MTB cells.  
93 These studies provide evidence to support the hypothesis that the vertical component of the GMF plays  
94 a role in determining the dominant polarity type among MTB in their natural habitats. As a result, the  
95 GMF serves as an essential reference frame that MTB rely on for navigation and migration in their  
96 native environments.

97

98 More recent study showed that the magnetic field (500 mT) could impact the magnetosome formation  
99 and antioxidant defense systems in *M. gryphiswaldense* MSR-1 (Leila et al., 2019). Our earlier studies  
100 have also found that applied 2 mT 50 Hz pulsed magnetic fields (PMFs) could promote magnetosome  
101 formation in *M. magneticum* AMB-1 cells (Pan et al., 2010). Interestingly, compared with 500 nT  
102 hypomagnetic field, the GMF significantly promoted the cell growth at stationary-phase but reduced  
103 cellular magnetism at exponential growth phase in *M. magneticum* AMB-1 (Wang et al., 2008). These  
104 results suggest that the GMF plays an important role in the biomineralization of magnetosome. Some  
105 studies on non-MTB (e.g., *Escherichia coli*) have shown that the application of a moderate static  
106 magnetic field (SMF) could impair the cell growth (Ji et al., 2009; Letuta et al., 2014; Li et al., 2022a).  
107 These indicate that the effect of magnetic field on microorganisms could be more intricate than  
108 previously assumed.

109

110 For a better understanding of the cellular and molecular mechanisms involved in the adaptation of  
111 MTB to GMF, we conducted microbiological, transcriptomic, and genetic experiments to analyze the

112 effects of weak SMF exposure on the cell growth and magnetosome formation in the MTB strain  
113 AMB-1. We observed that prolonged exposure to SMF had a significant impact on the cell growth and  
114 magnetosome formation of AMB-1. Furthermore, we analyzed the molecular mechanism of long-term  
115 SMF exposure in AMB-1 cells using transcriptome results and demonstrated that applying magnetic  
116 field stress altered the expression of vital genes involved in the sulfur metabolism pathway. By  
117 targeting the most downregulated differentially expressed genes (DEGs), specifically the  
118 adenylyl-sulfate kinase *cysC* gene in this pathway, we created an in-frame deletion mutant of *cysC* and  
119 assessed the effects on growth and magnetosome formation under SMF. These researches could  
120 contribute novel insights into the environmental adaptation mechanism of microorganisms and have  
121 potential applications in magnetic regulation.

122

## 123 **Materials and methods**

### 124 **Bacterial genetic manipulation**

125 Bacterial strains and plasmids used in this study are listed in Supplementary Table S1. Bacterial  
126 knockout mutant  $\Delta cysC$  in the AMB-1 background was constructed using the CRISPR-Cas9-based  
127 genome editing tool pCRISPOmyces-2 system (Chen et al., 2018; Cobb et al., 2015). The sgRNA was  
128 designed based on the target genes. The editing templates had a 1000 bp sequence homologous to each  
129 side (upstream or downstream) of the target genes. Once the target genes were deleted, the plasmid was  
130 cured to get the  $\Delta cysC$  knockout strain. For construction of the complementation strain, the *cysC*  
131 sequence was PCR amplified from AMB-1 and ligated into *EcoRI*- and *BamHI*-digested pAK0994.  
132 The complementing vector pAK*cysC* was assembled to complement  $\Delta cysC$ , named Com*cysC*, a  
133 pBBR1MCS-based plasmid carrying a kanamycin resistance gene and expressing the *cysC*-gfp fusion  
134 from a tac promoter. The method was performed as described previously (Chen et al., 2018). All  
135 plasmids were transformed into the *E. coli* strain WM3064 by chemical transformation and transferred  
136 into AMB-1 through biparental conjugation (Philippe and Wu, 2010). The mutant and complementary  
137 strains were verified by PCR and sequencing. The primers used in this study are listed in  
138 Supplementary Table S2.

139

### 140 **Bacterial culture and magnetic field treatment**

141 *M. magneticum* AMB-1 strains (ATCC700264) were grown on modified enriched magnetospirillum

142 growth medium (EMSGM) consisting of (per 1 L) 10 mL of Wolfe's vitamin solution, 5 mL of Wolfe's  
143 mineral solution, 2 mL of 0.01 M ferric quinate, 0.68 g of potassium phosphate, 0.12 g of sodium  
144 nitrate, 0.74 g of succinic acid, 0.05 g of L-Cys-HCl, 0.2 g of polypeptone, and 0.1 g of yeast extract  
145 (Yang et al., 2001).

146

147 Laboratory-built magnetic exposure apparatuses were composed of two groups of Helmholtz coils  
148 (experimental coil and control coil) and power supply, and were used to analyze the AMB-1 growth.  
149 Experimental coil pair of Helmholtz coils consisted of two identical coils, 180 turns each, separated by  
150 the radius of the coils. The current range generated by the power supply is 0 to 3 A, and the  
151 corresponding magnetic induction intensity in the central area ranges from 0 to 2.4 mT. The  
152 inhomogeneity of the SMF in the middle of the coils was less than 2% in a cubic space of 9 cm×9  
153 cm×9 cm. The magnetic induction intensity was measured using a Gaussmeter (Model 1500, CH-Hall  
154 Magnetic Technology Co., Ltd., Beijing, China). For the control coil, a pair of Helmholtz coils were  
155 double-wound, each containing 90 turns and the two windings with current in opposite directions.  
156 Since the currents in the two coils flowed in opposite direction, the magnetic field counteracted and the  
157 total magnetic strength was close to zero. The control and experimental coils generated the same  
158 amount of heat, which could exclude thermo-effect during magnetic field exposure. The biological  
159 effects of AMB-1 were analyzed by setting the intensity of SMF at 1.5 mT and the direction of SMF  
160 was vertically downward. The vertical, north–south, and east–west components of the GMF were  
161 measured as 32, 16, and 10  $\mu$ T, respectively, by a fluxgate magnetometer (Model CH-350, CH-Hall  
162 Magnetic Technology Co., Ltd., Beijing, China). All samples were placed in the center of the coils and  
163 incubated in the dark at 28-29°C for 20 h, as shown in Figure 1a.

164

#### 165 **Cell growth and magnetic response curves**

166 All strains were grown synchronously in EMSGM under microoxic conditions. After inoculation with  
167 bacteria at a starting optical density ( $OD_{600}$ ) of 0.02, all culture bottles were filled to 7/8 of their total  
168 volumes and tightly closed them with screw caps. Total 42 bottles were incubated at rest, 21 of them  
169 were in SMF and the other 21 bottles in GMF. Each bottle was used only once, opened at the time point  
170 indicated, for measuring  $OD_{600}$  and magnetic response ( $C_{mag}$ ). Therefore, the gradients of microoxic  
171 conditions in all bottles were established from AMB-1 metabolism without disturbance. Three bottles

172 were used to get an average value for each time point under SMF or GMF. The OD<sub>600</sub> was measured  
173 using a UV-visible spectrophotometer (UnicoUV-2800; UNICO Instrument Co., Shanghai, China). The  
174 C<sub>mag</sub> values were measured photometrically at 600 nm under a homogeneous 3 mT magnetic field, as  
175 described previously (Zhao et al., 2007). The OD<sub>600</sub> and C<sub>mag</sub> values were measured every 4 h, and  
176 OD<sub>600</sub> and C<sub>mag</sub> curves were constructed.

177

#### 178 **Cell growth with sulfate**

179 Experiments were performed to determine if the CysC which catalyzes the synthesis of activated  
180 sulfate is involved in growth and mineralization in AMB-1. WT,  $\Delta$ cysC, and ComcysC strains were  
181 cultured in EMSGM with cysteine or 0.4 mM Na<sub>2</sub>SO<sub>4</sub> replace cysteine for ~20 h, and WT strains were  
182 cultured in EMSGM (without sulfate) with added 10 mg/L, 15 mg/L, and 20 mg/L Na<sub>2</sub>SO<sub>4</sub> to the  
183 medium, and then OD and C<sub>mag</sub> were determined using a UV-Vis spectrophotometer at a wavelength  
184 of 600 nm. Sulfate concentrations were measured by ICS-1500 ion chromatography system (Thermo  
185 Fisher, USA).

186

#### 187 **Transmission electron microscopy**

188 The morphologies of AMB-1 cells were determined on a Hitachi-7700 transmission electron  
189 microscopy (TEM) system with an accelerating voltage of 80 kV. Briefly, the bacterial strains were  
190 grown in EMSGM at 28-29°C for 20 h until cell reached the stationary phase. AMB-1 cells were  
191 obtained and first suspended in water, drop-cast, and dried onto carbon-coated copper grids. The crystal  
192 sizes and shape factors were measured with ImageJ 1.51i software. The magnetosome sizes were  
193 defined as (length+width)/2. The shape factors were defined as width/length.

194

#### 195 **Analysis of magnetic properties**

196 Room-temperature hysteresis loops and first-order reversal curves (FORCs) measurements were  
197 performed on a MicroMag 3900 (Princeton Measurements Corporation, USA). The sensitivity of the  
198 magnetometer is  $5.0 \times 10^{-10}$  Am<sup>2</sup>. The hysteresis loops were measured between  $\pm 1.0$  T with an averaging  
199 time of 300 ms. Saturation magnetization ( $M_s$ ), saturation remanence ( $M_{rs}$ ) and coercivity ( $B_c$ ) were  
200 obtained from the hysteresis loop. The saturation isothermal remanent magnetization was measured at  
201 1.0 T, and coercivity of remanence ( $B_{cr}$ ) was determined from standard back-field measurements.

202 FORCs were measured by following the protocol described by Li et al., (2010). FORCs diagrams were  
203 calculated using the FORCinel version 1.05 software with a smoothing factor of 3. Low-temperature  
204 magnetic experiments were carried out on the dry cell samples using a quantum design MPMS XP-5  
205 magnetometer (sensitivity is  $5.0 \times 10^{-10}$  Am<sup>2</sup>). Zero-field-cooled (ZFC) and field-cooled (FC) curves  
206 were acquired by cooling the samples from 300 K to 5 K in a zero field and in a 5 T field, respectively,  
207 followed by giving a saturation isothermal remanent magnetization in a field of 5 T at 5 K (hereafter  
208 termed SIRM5T-5K), and then measuring the remanent magnetization in zero field at intervals of 2–5  
209 K upon warming to 300 K. The Verwey transition temperature ( $T_v$ ) was defined as the temperature for  
210 the maximum of the first-order derivative of the FC curve ( $dM/dT$ ) (Li et al., 2010; Pan et al., 2005).

211

### 212 **Transcriptomic analysis and quantitative real-time PCR assay**

213 The transcriptomic analyses were performed with cells in the stationary phase at 20 h.  
214 Total culture RNA was then extracted using the TIANGEN RNAPrep Pure Cell/Bacteria Kit. RNA  
215 quantities were assessed with agarose gel electrophoresis, NanoPhotometer® spectrophotometer  
216 (IMPLEN, CA, USA), and RNA Nano 6000 Assay Kit of the Bioanalyzer 2100 system (Agilent  
217 Technologies, CA, USA). cDNA libraries were then constructed and sequenced on an Illumina  
218 NovaSeq platform at Novogene Co., Ltd. (Beijing, China). High-quality RNA-Seq data (i.e., clean  
219 reads) were obtained by removing low-quality reads that contained (1) adapters, (2) more than 10%  
220 ambiguous nucleotides (N), and (3) more than 50% low-quality (Q-value  $\leq$  20) bases.

221

222 Expression levels were determined using several methods, including quantification of gene expression  
223 levels (HTSeq v0.9.1 software) and identification of DEGs using DESeq R (1.18.0). DESeq provides  
224 statistical routines for determining differential expressions in digital gene expression data using a  
225 model based on a negative binomial distribution. DEGs were defined based on the following criteria:  
226  $|\log_2(\text{foldchange})| > 1$  and  $P < 0.05$ . Gene Ontology (GO) enrichment analysis of the DEGs was  
227 conducted with the GOrseq R package, in which gene length biases were corrected. GO terms with  
228 corrected  $P$  values less than 0.05 were considered significantly enriched by the DEGs. The Kyoto  
229 Encyclopedia of Genes and Genomes (KEGG) orthology-based annotation system was used to test the  
230 statistical enrichment of the DEGs in the KEGG pathways. RNA-Seq data were deposited in the  
231 National Center for Biotechnology Information database under accession PRJNA852349.

232 Validation of RNA-seq data was performed using quantitative RT-PCR (RT-qPCR). The analysis was  
233 performed with cells grown under microoxic conditions, and the culture was prepared similarly to the  
234 method described above for measuring growth curves. Total RNA was extracted using an RNAPrep  
235 Pure Cell/Bacteria kit (Tiangen, China). Single-strand cDNA was synthesized with a reverse  
236 transcription kit (Takara, Japan). RT-qPCR assays were performed with the SYBR Green RT-PCR  
237 Mix (Thermo Fisher Scientific, USA) on an ABI QuantStudio 6 Flex RT-PCR System (Applied  
238 Biosystems, USA). The relative expression levels were calculated by the  $2^{-\Delta\Delta C_T}$  method and used the  
239 threshold cycle of *rpoD* for normalization (Chen et al., 2018). The experiment was repeated at least  
240 three times, with each sample run in triplicate. All primers used for probing each gene in this study are  
241 listed in Supplementary Table S2.

242

### 243 **Detection of ROS generation**

244 Intracellular ROS levels were analysed using the DCFH-DA method (He and Hader, 2002). WT,  $\Delta$ *cysC*,  
245 and *ComcysC* strains were cultured in EMSGM under SMF or GMF exposure at 28-29°C for ~20 h  
246 when the cells grew into the stationary growth phase. 10 mL collected cell suspension was resuspended  
247 in 1 mL fresh medium. DCFH-DA (final concentration 10  $\mu$ M) was added and reacted with cells for 30  
248 min at 37°C in the dark. The cells were centrifuged at 13,000 rpm for 3 min and washed thrice with a  
249 PBS buffer. The fluorescence of all samples was measured using a fluorescence spectrophotometer  
250 (Hitachi F-4500, Japan) at an excitation wavelength of 485 nm and emission wavelengths of 500–600  
251 nm.

252

### 253 **Statistical Analysis**

254 All statistical analyses were performed using SPSS 25.0 (SPSS, IBM, USA). All data are expressed as  
255 the means  $\pm$  standard deviations. The data of OD<sub>600</sub> and Cmag values were analyzed using repeated  
256 measures analysis of variance (ANOVA) for time course, and two-tailed Student's *t*-test for  
257 comparisons at each time. The sizes and shape factors of magnetosomes and the number of  
258 magnetosomes in a cell were analyzed using the Mann–Whitney U-test. In all cases, statistical tests  
259 were considered significant at  $P < 0.05$ .

260

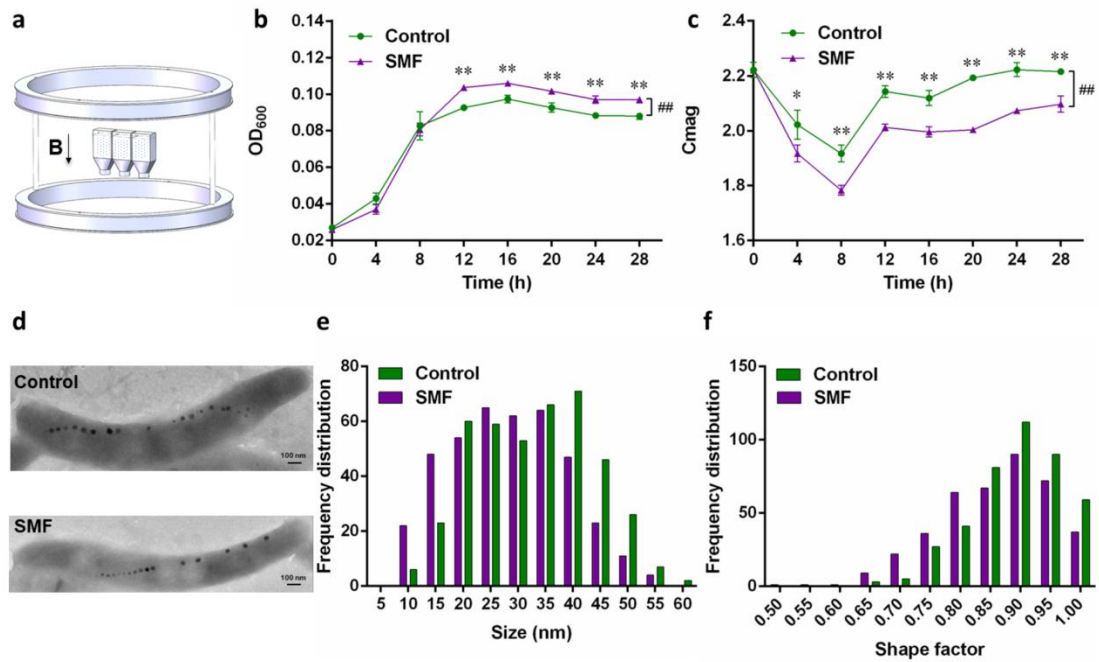
### 261 **Results**

262 **Effects of SMF on the cell growth and magnetosome formation in AMB-1**

263 To investigate the effects of SMF on bacterial growth and magnetosome mineralization, AMB-1 was  
264 exposed to SMF (1.5 mT) for 28 consecutive hours (Fig. 1a). The OD<sub>600</sub> and C<sub>mag</sub> were measured at  
265 600 nm. As the data show in Figure 1b, cells entered the exponential growth phase rapidly and reached  
266 stationary phase at 16 h and no significant differences were observed between SMF group and GMF  
267 group ( $P>0.05$ ) during initial exponential growth phase. Whereas after 12 h, the OD value of SMF  
268 group showed significantly higher than that of GMF control group ( $P<0.01$ ). This conclusion was  
269 corroborated by the repeated measure ANOVA ( $P<0.01$ ). For the whole C<sub>mag</sub> time course, the results  
270 revealed that the SMF significantly decreased the C<sub>mag</sub> values compared to the cultures incubated in  
271 the GMF ( $P<0.0001$ , Fig. 1c).

272

273 To verify the effect of the magnetic field on magnetosome formation, we further analyzed the sizes,  
274 shape factors, and numbers of magnetosomes in stationary growth phase of AMB-1 cells by TEM  
275 observations (Fig. 1d). Based on the TEM images, approximately 400 magnetosomes in 30 cells and 72  
276 cells for the magnetosomes particle numbers per cell were analyzed. The results showed that the  
277 particle numbers per cell in the SMF and GMF groups were comparable (Fig. S1,  $P>0.05$ ). However, the  
278 average size and shape factor of magnetic particles under SMF exposure ( $28.61\pm 10.40$  nm,  $0.85\pm 0.09$ )  
279 significantly differed from those under the GMF control exposure ( $32.77\pm 10.58$  nm,  $0.89\pm 0.08$ ,  $P<0.01$ ,  
280 Fig. 1e and f). The SMF group exhibits lower frequencies of single-domain magnetic particles and  
281 higher frequencies of superparamagnetic particles. These results were consistent with our observations  
282 of reduced C<sub>mag</sub> values. Thus, our data indicated that application of a moderate static magnetic field  
283 affected AMB-1 magnetosome formation.



284

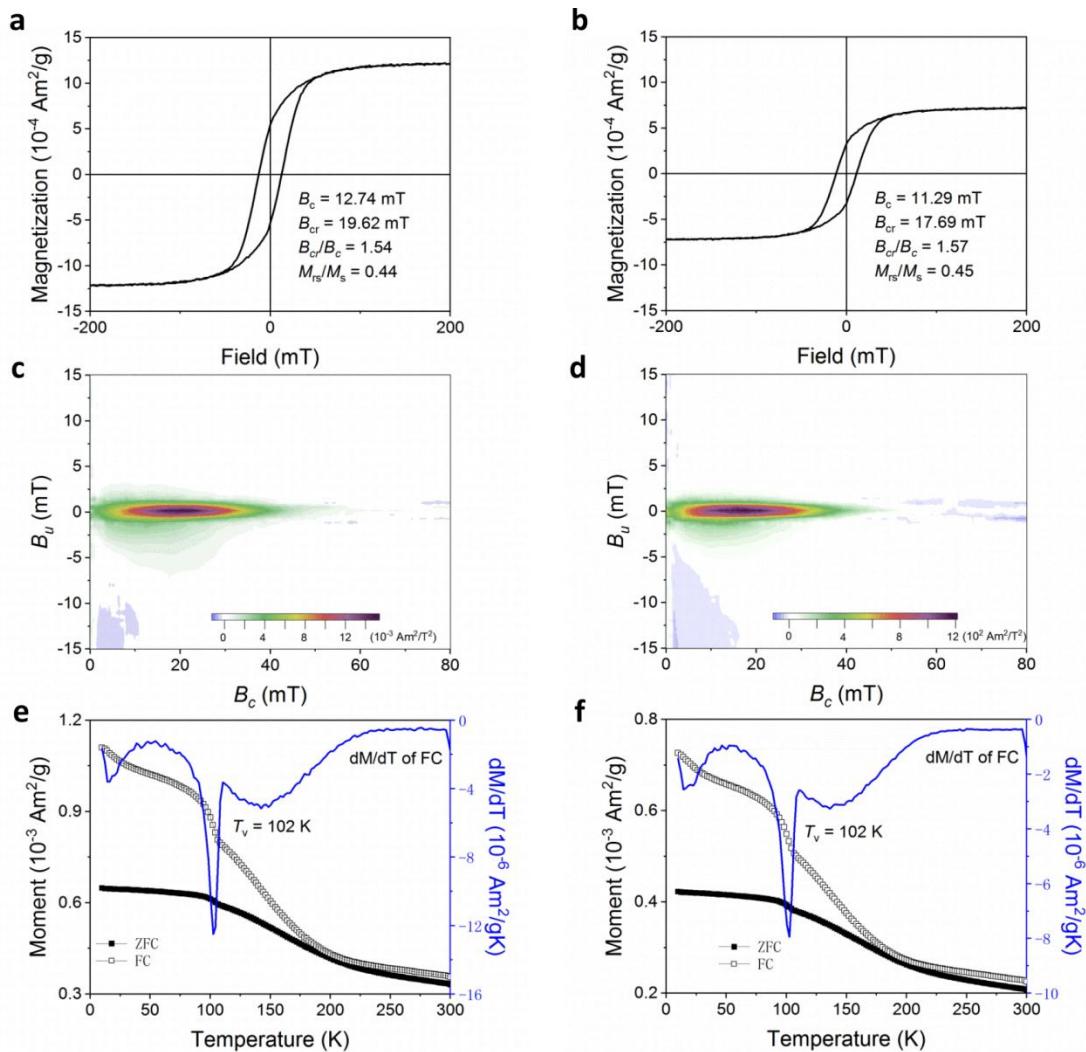
285 **Fig. 1.** AMB-1 cells cultured under 1.5 mT SMF and GMF control conditions and significant  
 286 differential cell growth and magnetosome mineralization under these two conditions. (a) Schematic of  
 287 the experimental setup: samples were placed in a custom-built pair of Helmholtz coils. (b) Cell growth  
 288 ( $n=3$ ) and (c) magnetic response  $C_{mag}$  curves ( $n=3$ ). (d) TEM observations at 20 h. Scale bars: 100 nm.  
 289 (e, f) Histogram analyses of the sizes and shape factors of magnetosomes under SMF ( $n=400$ ) and  
 290 GMF ( $n=419$ ) conditions in AMB-1 cells. The significant differences for time course of  $OD_{600}$  and  
 291  $C_{mag}$  are expressed in pound sign ( $##P<0.01$ ), statistical differences at the same time point are  
 292 indicated by one or two asterisks ( $*P<0.05$ ,  $**P<0.01$ ).

293

294 In addition, we further analyzed the magnetic properties of AMB-1 WT cells under SMF and GMF  
 295 treatments. Room-temperature hysteresis loops for these samples are shown in Figure 2a and b,  
 296 respectively. Both the hysteresis loops are closed at  $\sim 50$  mT, saturated at low field ( $<100$  mT) and well  
 297 characterized by the pot-bellied shape. The GMF cell sample shows typical Stoner-Wohlfarth type  
 298 hysteresis loop and has the  $B_c$ ,  $B_{cr}$ ,  $B_{cr}/B_c$  and  $M_{rs}/M_s$  values of 12.74 mT, 19.62 mT, 1.54 and 0.44,  
 299 respectively (Fig. 2a). In comparison, the SMF sample has the  $B_c$ ,  $B_{cr}$ ,  $B_{cr}/B_c$  and  $M_{rs}/M_s$  values of  
 300 11.29 mT, 17.69 mT, 1.57 and 0.45, respectively (Fig. 2b). The saturation magnetization of GMF  
 301 group ( $12.30 \times 10^{-4}$  Am<sup>2</sup>/g) was different from that of SMF group ( $7.22 \times 10^{-4}$  Am<sup>2</sup>/g). Generally, in a  
 302 FORC diagram, the horizontal axis  $B_c$  corresponds to the coercivity distribution and the vertical axis  $B_b$ ,

303 corresponds to the distribution of interaction fields. FORC diagrams for GMF and SMF treatment cells  
 304 showed smoothly closed concentric contours around a central peak, with peak coercivity of 21.38 mT  
 305 and 17.5 mT, respectively. Compared with the control group, SMF-treated cells slightly overlapped at  
 306 the  $B_b$  axis (Fig. 2c and d), indicating that fine-grained SD magnetosome particles were dominant, with  
 307 some SP magnetosome particles also present. The thermal demagnetization curves for the GMF and  
 308 SMF treatment cells are shown in Figure 2e and f, respectively. Both ZFC and FC curves show sharp  
 309 drops in remanence intensity between 90 K and 110 K, which corresponds to the Verwey transition of  
 310 magnetosome magnetite (Moskowitz and Egli, 2005; Moskowitz, 1993). Both samples have consistent  
 311  $T_v$  of 102 K, lower than ~120–125 K for stoichiometric magnetite. Taken together, these findings  
 312 suggest that SMF does not affect the chaining and magnetite properties of AMB-1 magnetosomes, but  
 313 may be affect the size of magetosomes as observed by TEM analysis (Fig. 1).

314



315

316 **Fig. 2.** Magnetic properties of AMB-1 WT cells cultured under 1.5 mT SMF and GMF control  
317 conditions. Room-temperature hysteresis loops, FORCs and low-temperature saturation remanence  
318 demagnetization curves of the whole AMB-1 GMF (a, c, e) and SMF (b, d, f) treated samples.

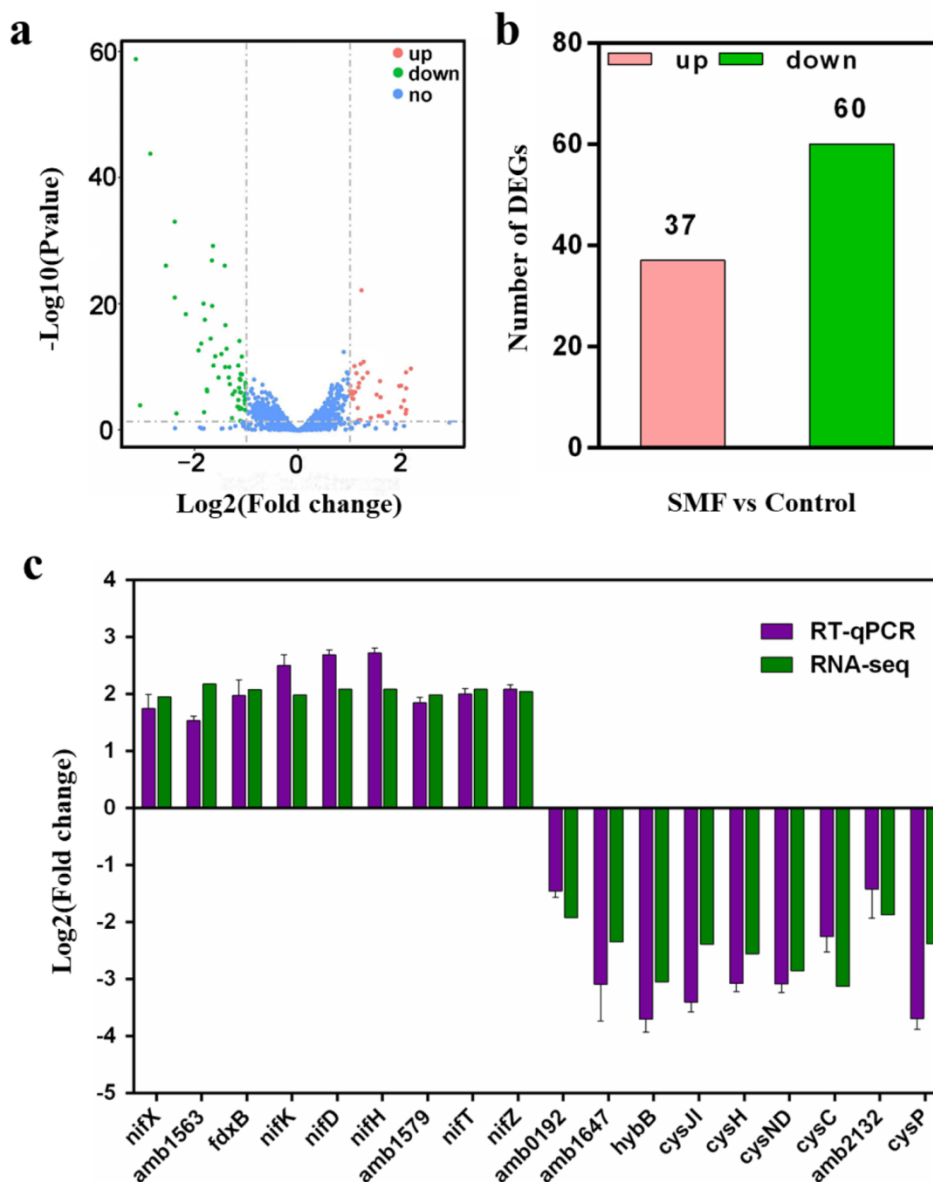
319

### 320 **Transcriptomic analysis of AMB-1 after SMF exposure**

321 To dissect the biological processes regulated by the SMF, we performed high-throughput  
322 transcriptomic analysis of bacteria treated with the GMF and with a 1.5 mT SMF for 20 h, showing that  
323 significant differences in growth and magnetosome mineralization (Fig. 1b and c). Three independent  
324 biological samples taken at 20 h of incubation were analyzed by RNA-Seq. As shown in Table S3, after  
325 quality filtering of raw reads with low quality, over  $1.48 \times 10^7$  clean reads with Q30 values over 92.59%  
326 of the sequence were obtained for all samples. Furthermore, over 98.77% of the clean reads were  
327 mapped to reference sequences, indicating successful library construction and RNA sequencing.

328

329 According to the comparative transcriptome results, a total of 4640 expressed genes were identified  
330 from all samples (Table S4). Among the expressed genes, 97 were DEGs when comparing the  
331 WT\_SMF and control groups ( $|\log_2(\text{fold change})| > 1$ ,  $P < 0.05$ ) with 30 up- and 67 downregulated (Fig.  
332 3a and b, Supplementary Table S5). Principal component analysis (PCA) showed that the SMF  
333 treatment altered the expression levels of AMB-1 genes (Fig. S2). The two main coordinates explained  
334 72.53% of the variation, of which PC1 explained 42.89% and PC2 explained 29.64%. The  
335 transcriptomic data were verified by RT-qPCR analysis of 18 randomly selected genes that were  
336 upregulated or downregulated in RNA-seq. In general, the qPCR results agreed with the transcriptomic  
337 data (Fig. 3c), which validated the transcriptomic data.



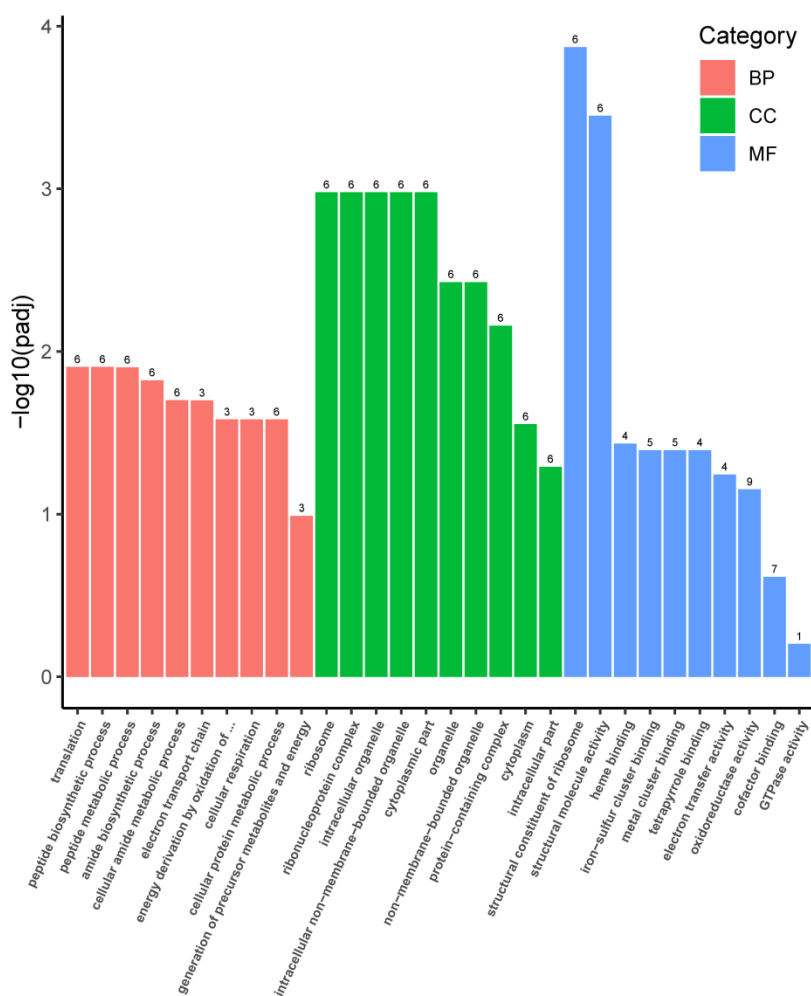
338

339 **Fig. 3.** AMB-1 cells cultured under SMF and GMF conditions and significant differentially expressed  
 340 genes under these two conditions. (a) Volcano plot of DEGs in AMB-1 cells. (b) Genes that passed the  
 341 statistical threshold were counted to determine the changes due to the SMF treatment. The pink column  
 342 represents the number of upregulated unigenes, and the green column represents the number of  
 343 downregulated unigenes. (c) Comparison of gene expression levels of RNA-seq and qRT-PCR.

344

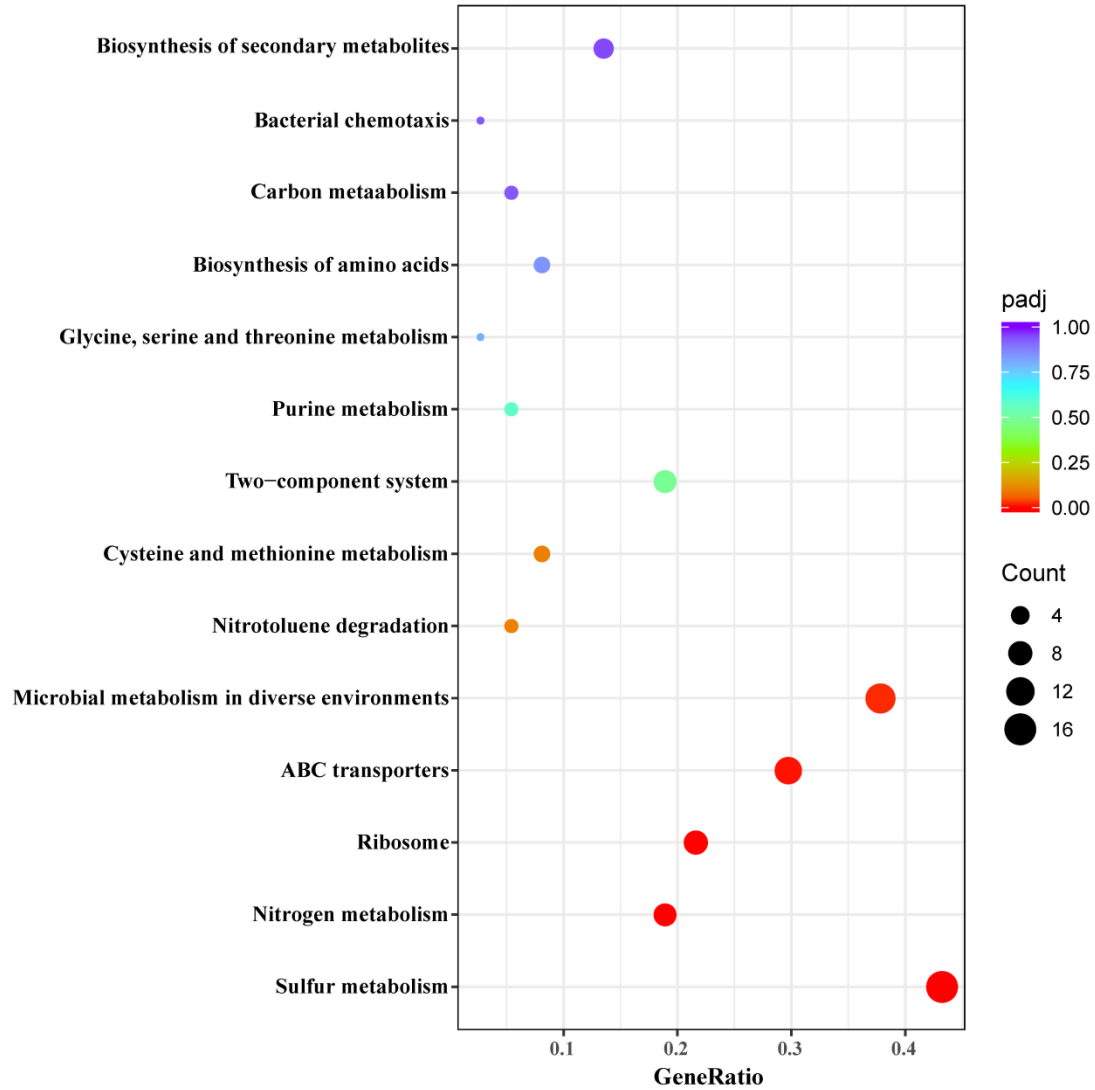
345 To better understand the functions, metabolic pathways and interactions of the DEGs associated with  
 346 SMF effects, GO and KEGG enrichment analyses were performed. A total of 139 GO terms were  
 347 assigned to 509 DEGs in AMB-1, including 73 biological process (BP) terms, 18 cellular component  
 348 (CC) terms, and 48 molecular function (MF) terms (Fig. 4). In addition, KEGG enrichment analysis

349 was further performed to classify the DEGs into different pathways, which could reveal the functional  
 350 information and relationships among these DEGs (Xie et al., 2011). KEGG analysis showed that a total  
 351 of 82 DEGs were involved in signaling pathways with 67 downregulated and 15 upregulated in  
 352 SMF-treated bacteria. Sulfur metabolism, nitrogen metabolism, ribosome, ABC transporters and  
 353 microbial metabolism in diverse environmental pathways were the most enriched pathways in the  
 354 DEGs, and other major pathways included nitrotoluene degradation, two-component system, and  
 355 biosynthesis of secondary metabolites, suggesting that these pathways played important roles in SMF  
 356 treatment (Fig. 5).



357  
 358 **Fig. 4.** DEGs were assigned GO to three categories: biological process (BP, red), cellular component  
 359 (CC, green) and molecular function (MF, blue).

360



361

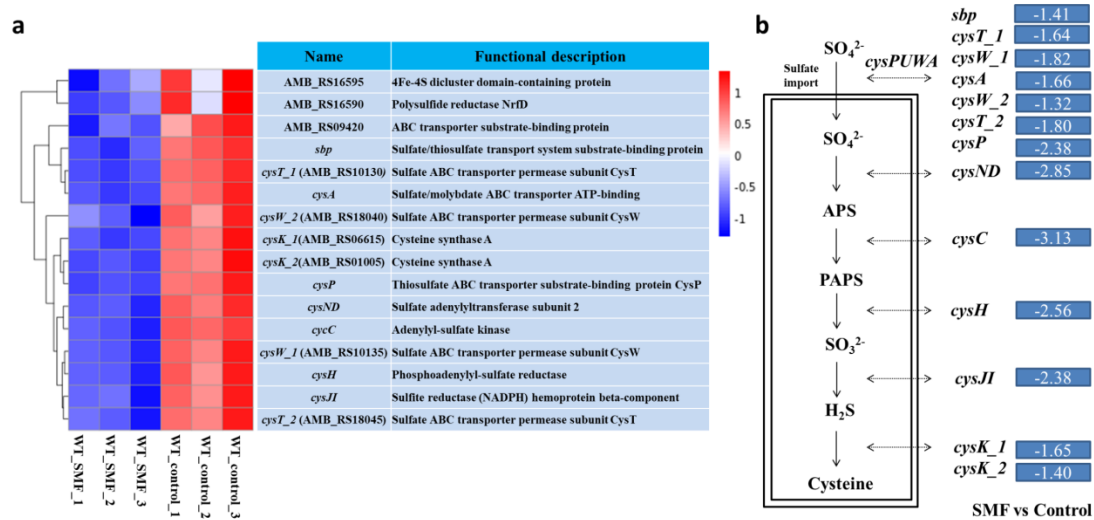
362 **Fig. 5.** KEGG enrichment analysis of DEGs. The size of the origin represents the number of genes  
 363 enriched in each pathway. Different colors represent different adjusted *P*-values.

364

365 **Effect of SMF on sulfur and nitrogen metabolism in AMB-1 cells**

366 KEGG provides a reference database for linking genomic or transcriptomic contents of genes to KEGG  
 367 reference pathways and to thereby infer systemic behaviors of cells. Based on genome analysis, The  
 368 KEGG pathway database (<https://www.kegg.jp/pathway/mag00920>) shows the complete sulfur  
 369 metabolism of AMB-1 cells. Our transcriptome results showed the highest degree of enrichment for  
 370 sulfur metabolism. The CysPUWA transporter is known to mediate sulfate transport into cells in an  
 371 ATP-dependent manner (Aguilar-Barajas et al., 2011; Goff and Yee, 2017). The subsequent step is  
 372 assimilatory sulfate reduction, which may convert sulfate into new biomass. Sulfate is reduced via the

373 classic assimilatory sulfate reduction route, involving a series of enzymes including ATP sulfurylase  
 374 (sulfate adenylyl-transferase, CysND), adenylyl-sulfate kinase (CycC), phosphoadenosine  
 375 phosphosulfate reductase (CysH), and a one-subunit cyanobacterial-type ferredoxin-sulfite reductase  
 376 (CysJI) (Li and Bao 2021). Our results showed 16 of the 97 DEGs (*cysC/cysND/cysP/cysT/cysA/cysH/  
 377 sbp/cysJI/cysW\_1/AMB\_RS06615/cysT/cysK\_1/cysK\_2/cysW\_2/AMB\_RS16595/AMB\_RS16590*)  
 378 participated in assimilatory sulfate reduction, and all were downregulated under SMF conditions (Fig.  
 379 6).



380  
 381 **Fig. 6.** Analysis of DEGs associated with sulfate metabolism in AMB-1 with and without SMF  
 382 treatment. (a) Heatmap of typical DEGs associated with sulfate metabolism. Red indicates upregulated  
 383 genes, while blue indicates downregulated genes. (b) Conceptual diagram of assimilatory sulfate  
 384 reduction and related changes in gene expression.

385  
 386 Earlier studies found that MTB have evolved the ability to reduce  $N_2$  to generate  $NH_3$  in a process  
 387 known as biological nitrogen fixation (Bazyliński et al., 2000; Jiang et al., 2002). Genomic analysis  
 388 identified complete dissimilatory nitrate reduction and denitrification pathways in AMB-1 (Fig. S3).  
 389 Our results showed that a total of 15 DEGs encoded nitrogen metabolism systems. Three nitrogen  
 390 fixation pathway genes (e.g., *nifD/nifK/nifH*) and eight putative or associated nitrogen fixation genes  
 391 (e.g., *AMB\_RS07895/nifT/nifQ/nifX/nifB/AMB\_RS00080/nifZ/fdxB*) were upregulated under SMF  
 392 conditions. Among them, *nifD* and *nifK*, encoding the nitrogenase that catalyzes the fixation of  $N_2$  to  
 393  $NH_3$ ; *nifH*, encoding nitrogenase reductase; and *nifZ* and *nifT* exhibited 4.26-, 3.97-, 4.25-, 4.13-, and  
 394 4.25-fold upregulations in their expressions, respectively. Furthermore, three ABC transporter genes

395 (e.g., AMB\_RS02760/AMB\_RS02765/AMB\_RS02755) belonged to the nitrogen metabolism pathway,  
396 and each was upregulated under SMF conditions (Fig. S4).

397

398 In addition, we noticed that the SMF significantly downregulated the mRNA level of cytochrome bc. A  
399 previous study showed that cytochrome c peroxidases are diheme enzymes required for the reduction  
400 of H<sub>2</sub>O<sub>2</sub> to water in bacteria (Wolf et al., 2018). The SMF treatment also significantly downregulated  
401 the mRNA levels of *hybA* (3.52-fold), which encodes the hydrogenase 2 and *hybB* (8.25-fold), which  
402 encodes the Ni/Fe-hydrogenase cytochrome b subunit. Interestingly, several genes involved in iron  
403 transport (e.g., AMB\_RS04825 and AMB\_RS04830) were downregulated by the SMF treatment,  
404 suggesting that iron metabolism system is involved in magnetic field regulation, which may influence  
405 iron mineralization in vivo. Considering these results together, our data imply that SMF treatment  
406 affects bacterial growth and magnetosome mineralization, probably with the assistance of ribosome,  
407 cytochrome, and iron transport systems.

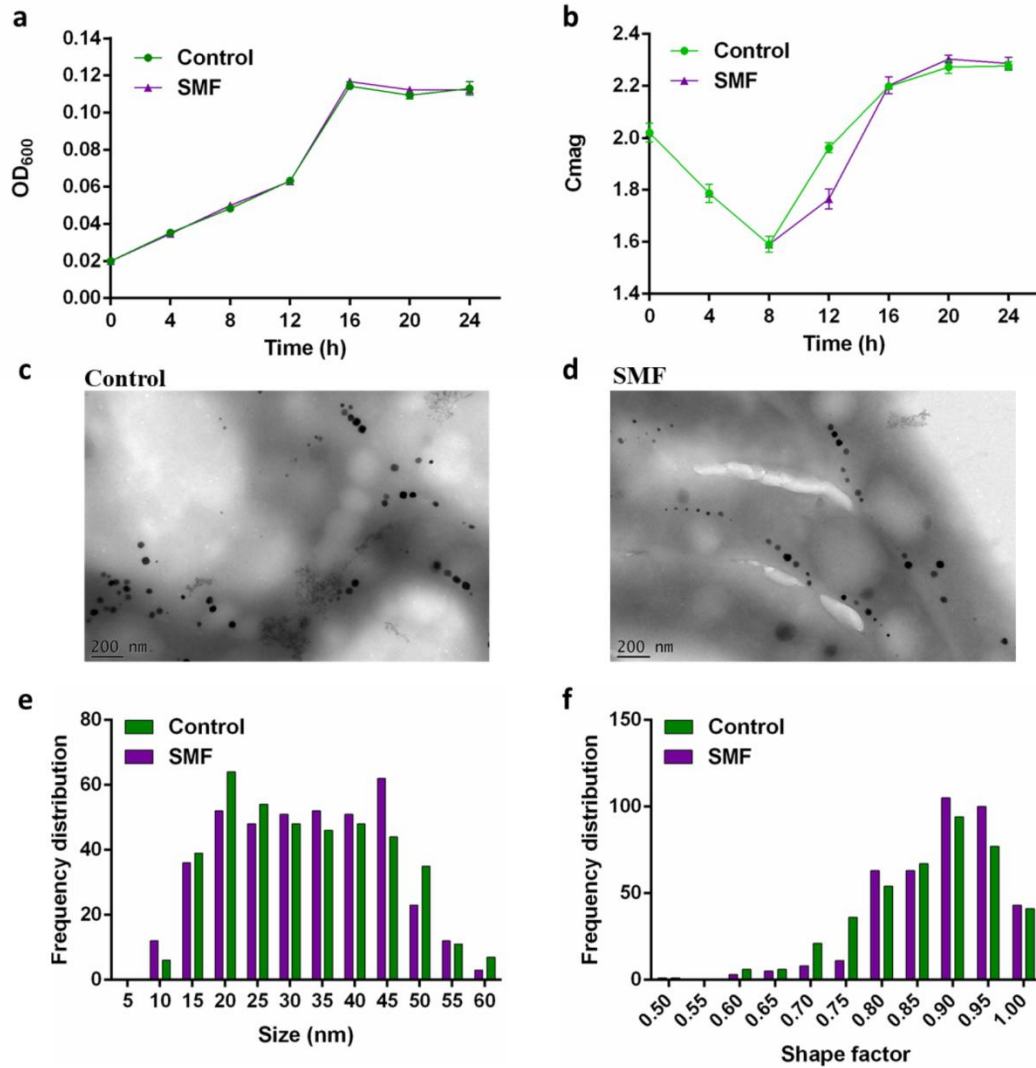
408

#### 409 **SMF affects AMB-1 growth and mineralization through repressing *cysC* expression**

410 Based on our RNA-seq data showing that *cysC* was the most downregulated DEGs by SMF, we  
411 proposed that SMF probably effects cell growth and mineralization via the sulfur metabolism bypass.  
412 To investigate the role of *cysC*, we performed a CRISPR-Cas9-based gene knockout experiment to  
413 construct in-frame deletion of *cysC*. The effects of SMF-treated on cell growth and Cmag values in  
414  $\Delta cysC$  mutant were analysed.

415

416 As shown in Figure 7a and b, the OD and Cmag curves were similar between SMF-treated and  
417 GMF-treated cultures, suggesting that knockout *cysC* is insensitive to SMF. Meanwhile, our TEM  
418 results also showed that the average size of magnetic particles in the SMF (32.25±11.76 nm) and GMF  
419 (32.37±12.22 nm) groups was not affected (Fig. 7c, d and e). In contrast with AMB-1 WT strain, the  
420 difference of magnetosomes shape factor between SMF and GMF exposure in the mutant was reduced  
421 (Fig. 7f). Thus, our data suggest that the *cysC*, as a key gene, can participate in the cells growth and  
422 mineralization in AMB-1 by SMF regulation.



423

424 **Fig. 7.** Cells growth and magnetosome mineralization for  $\Delta cysC$  mutant cells cultured under 1.5 mT

425 SMF and GMF control conditions. (a) Cell growth ( $n=3$ ) and (b) magnetic response  $C_{mag}$  curves ( $n=3$ ).

426 (c, d) TEM observations at 20 h. Scale bars: 200 nm. (e, f) Histogram analyses of the sizes and shape

427 factors of magnetosomes under SMF ( $n=402$ ) and GMF ( $n=403$ ) conditions in  $\Delta cysC$  mutant cells.

428

#### 429 Analysis of sulfur source utilization of *cysC* deletion mutant in the presence and absence of SMF

430 To elucidate the CysC function, we analysed the effect of SMF treated on cell growth and

431 mineralization under sulfur source utilization in AMB-1 WT,  $\Delta cysC$  and *ComcysC* that was  $\Delta cysC$

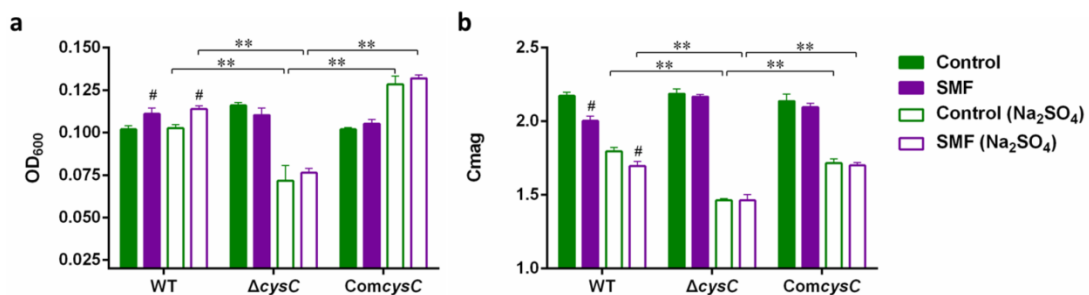
432 mutant complemented by plasmid pAKcysC expressing the CysC-GFP fusion protein. These strains

433 were incubated in liquid media supplemented with sulfate ( $Na_2SO_4$ ), instead of cysteine, for 20 h in

434 stationary growth phase. For AMB-1 WT, the SMF significantly increased the cell growth ( $P<0.05$  and

435  $P<0.01$ ) but decreased  $C_{mag}$  values ( $P<0.01$  and  $P<0.05$ ) under the two conditions of cysteine and

436 Na<sub>2</sub>SO<sub>4</sub> as sulfur sources. However, the difference in bacterial growth and Cmag between SMF-treated  
 437 and untreated bacteria was disappeared for mutants in these two cultured conditions (Fig. 8,  $P>0.05$ ),  
 438 suggesting that sulfate import of assimilative sulfate reduction pathway is specific for AMB-1  
 439 adaptation to the SMF stimulus. For strains in Na<sub>2</sub>SO<sub>4</sub> cultured condition, the values of OD and Cmag  
 440 in WT and ComcysC were significantly higher ( $P<0.01$ ) than that of  $\Delta$ cysC strain, demonstrating that  
 441 cysC may be a key gene in assimilative sulfate reduction, which can convert sulfate into new biomass.  
 442 However, our results showed that there was no significant difference in OD or Cmag values in the  
 443 complemented mutant group when grown in SMF and GMF conditions, although their average values  
 444 variation trends were consistent with those of the WT strains. To explain this, the relative abundance of  
 445 CysC-GFP in ComcysC cells was checked with a fluorescence microscope. Statistical results showed  
 446 that approximately 38% of cells did not express the protein (Fig. S5). The low level of fluorescence  
 447 observed may be due to plasmid instability, as well as poor heterogeneous expression of cysC-gfp from  
 448 the pBBR1MCS vector. Collectively, these factors suggest partial complementation of  $\Delta$ cysC in  
 449 ComcysC. Taken together, our findings suggest that CysC may serve as a pivotal enzyme in mediating  
 450 sulfur metabolism to synchronize the impact of SMF on both growth and magnetization of AMB-1.



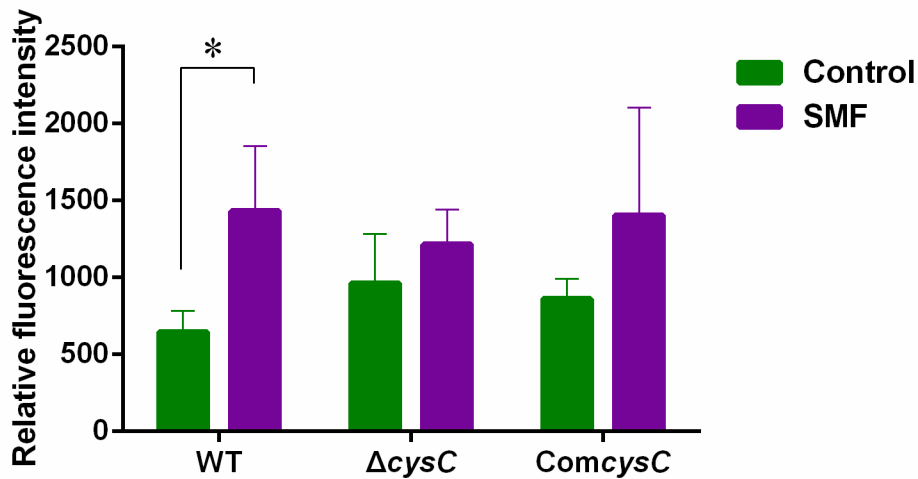
451  
 452 **Fig. 8.** The growth (a) and Cmag (b) values under 1.5 mT SMF and/or by adding Na<sub>2</sub>SO<sub>4</sub> to the  
 453 medium ( $n=3$ ). Level of significance of the differences observed between SMF and GMF control is  
 454 expressed in pound sign ( $\#P<0.05$ ). The significant differences between the two groups depicted by the  
 455 lines in the graph are indicated by one or two asterisks ( $*P<0.05$ ,  $**P<0.01$ ).

456

#### 457 SMF regulates cysC gene to affect the intracellular ROS level

458 To understand the mechanism by which cysC is involved in affecting cell growth and magnetosomes  
 459 synthesis under magnetic field, we further examined intracellular ROS levels by the DCFH-DA method  
 460 for WT,  $\Delta$ cysC and ComcysC cells (Fig. 9), because sulfur metabolism pathway might influence ROS

461 levels to maintain redox homeostasis (Balasubramanian et al., 2022). The ROS levels of WT in  
462 SMF-treated cells were significantly higher than those of control cells ( $P<0.05$ ), whereas the ROS level  
463 no significantly increased in mutant cells and complemented cells ( $P>0.05$ ). Regarding the observed  
464 changes in Cmag values under SMF, *cysC* gene may be involved in regulating expression levels of  
465 cellular magnetosome synthesis probably to coordinate the effects on intracellular ROS.



466  
467 **Fig. 9** Effects of CysC on intracellular ROS level in AMB-1 cells ( $n=3$ ). The level of significance of  
468 the differences observed between the SMF and GMF control is expressed as asterisks ( $*P<0.05$ ).  
469

## 470 Discussion

471 In this study, we found that the 1.5 mT SMF treatment promoted the cell growth but reduced  
472 magnetosome formation in AMB-1. This phenotypic change trend seems to be consistent with the  
473 results that the biomass at stationary-phase in GMF was higher and cellular magnetism at exponential  
474 growth phase was lower than that of bacteria cultivated in hypomagnetic field (Wang et al., 2008). This  
475 was different from our previous results using PMFs, where 2 mT PMFs stimulated magnetosome  
476 formation in AMB-1, while growth remained unaltered (Pan et al., 2010). It could be the general  
477 difference between SMF and dynamic/time-varying magnetic field. PMFs could apply a peak magnetic  
478 density with a useful level for a short period of time, but a constant application of such high density  
479 might have different effects on cell growth compared to a SMF. The induced electric field due to the  
480 changed magnetic field maybe also a key factor that causes these differences. [Moreover, the results of  
481 the TEM observations and magnetic properties showed that the mineralizing ability of magnetosomes  
482 in SMF group was significantly weaker than that in GMF group.](#) Taken together, these results suggest

483 that lower strength of SMF has significant effects on bacterial cell growth and biommineralization of  
484 magnetosomes, and tend to produce smaller magnetosomes. It is physically meaningful that when a  
485 magnetic field higher than the GMF is applied, less magnetic moment of the MTB is required for cells  
486 to align along stronger field lines. As a consequence, AMB-1 only needs to synthesize relatively small  
487 magnetosomes to swim along the magnetic field and find the most suitable ecological niche. In  
488 addition, SMF treatment slightly increased the growth rate of WT AMB-1 at the later stage of  
489 exponential growth. However, some studies have shown that a weak magnetic field in the range of 0.5  
490 to 600 micro-Tesla can both increase and decrease the growth rate of bacteria (Filipic et al., 2012;  
491 Masood and Samina, 2017; Masood et al., 2020). It could be that different magnetic fields have  
492 different effects on bacterial growth patterns, depending on the strain of bacteria.

493

494 Transcriptomic analysis revealed that the effects of SMF-treated AMB-1 cells on growth and  $C_{mag}$   
495 values were closely related to downregulated expression of sulfur metabolism pathway. In sulfur  
496 metabolism, sulfate import genes *cysPUWA* and the assimilatory sulfate reduction genes were  
497 downregulated under exposure to a magnetic field. These genes encode enzymes involved in multiple  
498 steps of assimilating sulfate reduction and thereby maintain the normal physiological metabolism (Li  
499 and Bao, 2021). We investigated whether the enhanced growth of SMF-treated cells could cause faster  
500 depletion of sulfate in the medium, leading to downregulation of the sulfate assimilation pathway. Our  
501 measurements of sulfate concentrations after 20 h of treatment showed no significant difference  
502 ( $P>0.05$ ) in residual concentration of  $SO_4^{2-}$  in the medium between the SMF-treated and untreated  
503 cultures (Table S6). Our results also confirmed that SMF treatment promoted cell growth but reduced  
504 magnetosome formation in AMB-1 for all cultures with the addition of sulfate (Fig. S6). These results  
505 rule out the eventual indirect effect that may arise due to faster sulfate consumption in the cultures. Our  
506 subsequent assays with genetic and physiological approaches confirmed the role of *cysC* in  
507 SMF-treated cell growth increase and magnetosome formation inhibition. First, the null  $\Delta cysC$  mutant  
508 was not sensitive to 1.5 mT SMF. Second, the addition of either the cysteine or  $Na_2SO_4$  as sulfur source  
509 to the liquid medium successfully removed the effect of SMF on bacterial growth and  $C_{mag}$  values,  
510 suggesting that sulfate metabolism play a key role for bacteria in SMF exposure. Additionally, sulfur  
511 metabolism may directly supply elemental S for iron-sulfur (Fe-S) cluster biosynthesis (Roche et al.,

512 2013). Thus, our data imply that SMF treatment probably affects bacterial growth via the sulfur  
513 metabolism pathway, which has been demonstrated to play an important role in bacterial adaptation.

514

515 ROS can be generated by various cellular processes and the specific genes involved in the response to  
516 ROS may differ depending on the source of ROS and the bacterial strain. In this study, we found that  
517 the ROS levels of WT cells under a SMF condition were significantly higher than those of control cells,  
518 while the ROS levels of the mutant strain were not affected by the magnetic field. The mechanism by  
519 which SMF treatment induces intracellular ROS levels in WT AMB-1 is not fully understood. Previous  
520 studies have explored the effects of SMF on ROS levels and have shown that SMF can affect charged  
521 ROS molecules such as superoxide anion ( $\bullet\text{O}_2^-$ ), hydroxyl radical ( $\bullet\text{OH}$ ), and single oxygen ( $^1\text{O}_2$ )  
522 (Wang and Zhang, 2017). The most well-known example of this is the free radical pair mechanism  
523 involved in geomagnetic navigation (Ritz et al., 2000; Xu et al., 2016; Zadeh-Haghighi and Simon,  
524 2022). One explanation is that SMF affect the state of charged free radicals and thus affect intracellular  
525 ROS levels. Additionally, it is possible that the observed increase in ROS levels was the involvement of  
526 magnetosomes, which are intracellular iron nanocrystals synthesized by MTB (Spring and Bazylinski,  
527 2002). Redox modulation has been found to play a critical role in magnetosome formation (Bazylinski  
528 and Blakemore, 1983; Chen et al., 2020a; Chen et al., 2020b; Guo et al., 2012; Leila et al., 2019; Li et  
529 al., 2017), and studies have shown that magnetosomes can scavenge ROS and exhibit peroxidase  
530 activity (Guo et al., 2012; Li et al., 2017). Further, magnetosomes have been implicated in Fenton-like  
531 processes (Li et al., 2017). SMF possibly indirectly regulates intracellular ROS levels by influencing  
532 the Fenton reaction rate or peroxidase activity of magnetosomes. Thus, it is speculated that SMF may  
533 influence downstream signaling pathways, gene expression, enzyme activity of magnetosomes, and  
534 ultimately, cellular fate, either by directly generating free radicals or ROS.

535

536 Furthermore, the SMF treatment was observed to decrease magnetite crystal size and cellular  
537 magnetism in WT AMB-1. However, the cells lost sensitivity to SMF when the *cysC* gene was deleted.  
538 This suggests a feedback regulatory mechanism where ROS elevation caused by cellular sulfur  
539 metabolism indirectly balances the overall intracellular ROS level by influencing magnetosome size.

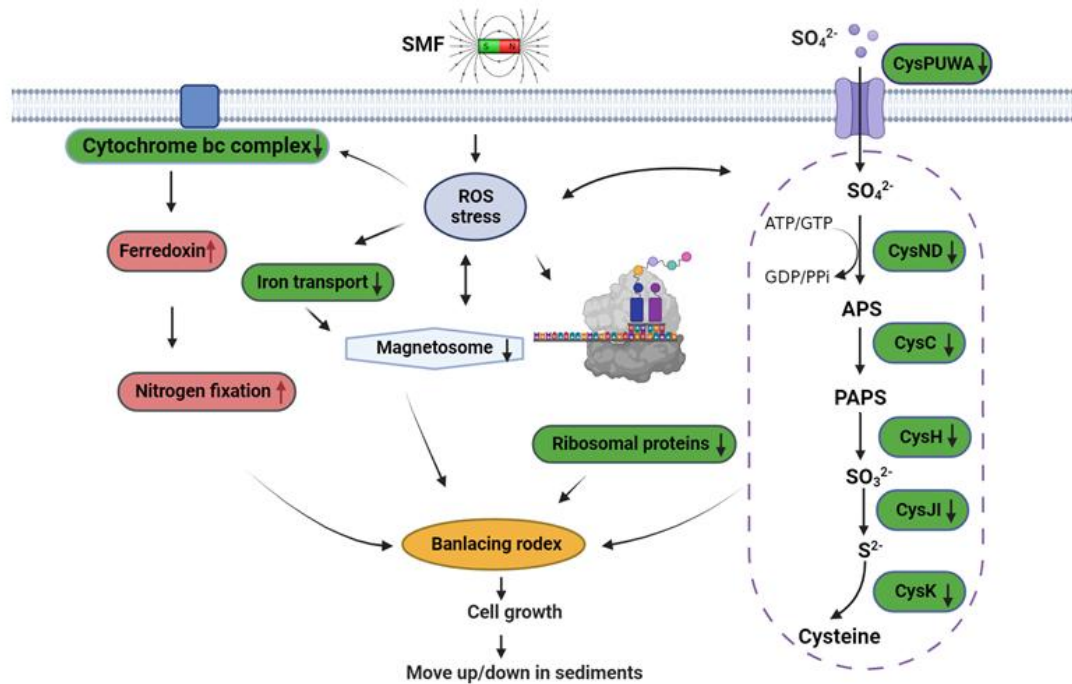
540 CysC may be involved in signaling pathways or regulatory mechanisms that are affected by SMF and  
541 may regulate the expression of cellular magnetosome synthesis. This indicates a complex relationship  
542 between cellular metabolism, magnetosome synthesis, and ROS. The mineralizing pathways of  
543 magnetosomes involved in redox equilibrium can be affected by SMF treatment, potentially negating  
544 any growth benefits gained solely by reducing oxidative stress. In addition, it is worth noting that the  
545 presence of numerous oscillating systems in the growth of bacteria contributes to both an increase and  
546 a decrease in oxidative stress, and these systems involve feedback with time delays. This suggests that  
547 bacteria have multiple mechanisms to regulate their levels of oxidative stress. To fully comprehend the  
548 underlying mechanisms, it is necessary to conduct more thorough investigations into the intricate  
549 relationship between SMF and redox equilibrium, levels of ROS, growth and mineralization of MTB.

550 Recently, several studies have shown that *Candidatus Magnetobacterium casensis* cells may efficiently  
551 shuttle nitrate downward for reduction and sulfur upward for oxidation by geomagnetically guided  
552 up-down movements within the oxic-anoxic transition zone (OATZ) (Li et al., 2021a). Our results  
553 suggesting that magnetic fields mainly affect the sulfur and nitrogen metabolism of cells through ROS,  
554 which indirectly affect the redox sites of the medium. It is possible that changes in the relative  
555 expression levels of the functional genes in nitrogen and sulfur metabolism indicated that these shifts  
556 may have impacts on microbial adaptive behavior, ultimately reflected in MTB growth and  
557 biomineralization. Some studies have also demonstrated that nitrogen metabolism nitrate reductase Nap  
558 participates in redox reactions required for magnetite biomineralization in MSR-1 (Li et al., 2012); and  
559 c-type cytochromes participate in enzymatic iron reduction in MTB and thus in the control of cellular  
560 redox (Li, 2021b). Our study showed that cytochrome bc, the hydrogenase 2, the Ni/Fe-hydrogenase  
561 cytochrome b subunit and iron transport genes were downregulated, while the nitrate reductase *nirBD*  
562 gene was upregulated by the SMF treatment. It is possible that these genes modulate cellular redox  
563 status to help MTB find aquatic OATZ environments.

564

565 In summary, based on this study, we propose a possible explanation for the effects of SMF on AMB-1  
566 cell growth and magnetosome mineralization (Fig. 10). When a magnetic field is applied, SMF may  
567 trigger bacterial oxidative stress to regulate expression levels of the functional genes in sulfur and  
568 nitrogen metabolism. Additionally, the size of magnetosomes may be influenced by SMF, which could

569 also be correlated with levels of ROS. The reversible and complex interaction between magnetosomes  
 570 and ROS helps maintain the redox state in the body, ultimately affecting cell growth. These processes  
 571 likely then influence microbial adaptive behavior to help MTB find an aquatic OATZ environment.  
 572 These findings provide a new idea for the biological adaptation mechanisms of magnetic field  
 573 participation and for better understanding the biomineralization process and biogeochemical cycles in  
 574 prokaryotic systems.



575  
 576 **Fig. 10** Model of AMB-1 response to the SMF. Red and green boxes correspond to upregulated and  
 577 downregulated genes, respectively.

578  
 579

580 **Acknowledgements**

581 We thank Yan Liu (Institute of Geology and Geophysics, Chinese Academy of Sciences) for the  
 582 assistance of the measurement of magnetic properties.

583

584 **Conflict of interest**

585 The authors declare that they have no known competing financial interests or personal relationships  
 586 that could have appeared to influence the work reported in this paper.

587

588 **Ethical Statement**

589 This article does not contain any studies with human participants or animals performed by any of the  
590 authors.

591

592 **Funding**

593 This work was supported by the National Natural Science Foundation of China (nos. 51937011,  
594 32100031, 32071237, 51907192).

595

596 **Author contributions**

597 Haitao Chen (Conceptualization, Data curation, Formal analysis, Funding acquisition, Investigation,  
598 Methodology, Validation, Visualization, Writing-original draft, Writing-review & editing), Hongkai  
599 Shi (Data curation, Formal analysis, Investigation, Methodology, Validation, Visualization), Changyou  
600 Chen (Conceptualization, Funding acquisition, Supervision, Writing-review & editing), Yangkun Jiao  
601 (Methodology, Resources, Writing-review & editing), Pingping Wang (Conceptualization, Resources,  
602 Supervision, Writing-review & editing), Chuanfang Chen (Conceptualization, Resources, Funding  
603 acquisition, Writing-review & editing), Jinhua Li (Conceptualization, Data curation, Methodology,  
604 Project administration, Resources, Writing-review & editing), Long-Fei Wu (Conceptualization, Data  
605 curation, Funding acquisition, Methodology, Project administration, Resources, Supervision,  
606 Validation, Writing-review & editing), and Tao Song (Conceptualization, Data curation, Funding  
607 acquisition, Methodology, Project administration, Resources, Supervision, Validation, Writing-review  
608 & editing)

609

610 **Data Availability**

611 Data will be made available on request.

612

613 **References**

614 Aguilar-Barajas, E., Diaz-Perez, C., Ramirez-Diaz, M.I., Riveros-Rosas, H., Cervantes, C., 2011.

615 Bacterial transport of sulfate, molybdate, and related oxyanions. *Biometals* 24, 687-707.  
616 <https://doi.org/10.1007/s10534-011-9421-x>.

617 Balasubramanian, R., Hori, K., Shimizu, T., Kasamatsu, S., Okamura, K., Tanaka, K., Ihara, H.,  
618 Masuda, S., 2022. The sulfide-responsive SqrR/BigR homologous regulator YgaV of  
619 *Escherichia coli* controls expression of anaerobic respiratory genes and antibiotic tolerance.  
620 *Antioxidants* 11, 2359. <https://doi.org/10.3390/antiox11122359>.

621 Bazylinski, D.A., Blakemore, R.P., 1983. Denitrification and assimilatory nitrate reduction in  
622 *Aquaspirillum magnetotacticum*. *Appl. Environ. Microbiol.* 46:1118-1124. [https://doi.org/](https://doi.org/10.1128/aem.46.5.1118-1124.1983)  
623 [10.1128/aem.46.5.1118-1124.1983](https://doi.org/10.1128/aem.46.5.1118-1124.1983).

624 Bazylinski, D.A., Dean, A.J., Schüler, D., Phillips, E.J.P., Lovley, D.R., 2000. N<sub>2</sub>-dependent growth  
625 and nitrogenase activity in the metal-metabolizing bacteria, *Geobacter* and *Magnetospirillum*  
626 species. *Environ. Microbiol.* 2, 266-273. <https://doi.org/10.1046/j.1462-2920.2000.00096.x>.

627 Bazylinski, D.A., Frankel, R.B., 2004. Magnetosome formation in prokaryotes. *Nat. Rev. Microbiol.* 2,  
628 217-230. <https://doi.org/10.1038/nrmicro842>.

629 Chakraborty, S., Andersen, K.H., Visser, A.W., Inomura, K., Follows, M.J., Riemann, L., 2021.  
630 Quantifying nitrogen fixation by heterotrophic bacteria in sinking marine particles. *Nat.*  
631 *Commun.* 12. <https://doi.org/10.1038/s41467-021-23875-6>.

632 Chen, H.T., Li, D.D., Cai, Y., Wu, L-F., Song, T., 2020a. Bacteriophytochrome from *Magnetospirillum*  
633 *magneticum* affects phototactic behavior in response to light. *FEMS Microbiol. Lett.* 367.  
634 <https://doi.org/10.1093/femsle/fnaa142>.

635 Chen, H.T., Li, J.H., Xing, X., Du, Z.J., Chen, G.J., 2015. Unexpected diversity of magnetococci in  
636 intertidal sediments of Xiaoshi island in the North Yellow Sea. *J. Nanomater* 2015  
637 <https://doi.org/10.1155/2015/902121>.

638 Chen, H.T., Li, K.F., Cai, Y., Wang, P.P., Gong, W.M., Wu, L-F., Song, T., 2020b. Light regulation of  
639 resistance to oxidative damage and magnetic crystal biogenesis in *Magnetospirillum*  
640 *magneticum* mediated by a Cys-less LOV-like protein. *Appl. Microbiol. Biot.* 104, 7927-7941.  
641 <https://doi.org/10.1007/s00253-020-10807-5>.

642 Chen, H.T., Zhang, S-D., Chen, L.J., Cai, Y., Zhang, W.J., Song, T., Wu, L-F., 2018. Efficient genome  
643 editing of *Magnetospirillum magneticum* AMB-1 by CRISPR-Case9 system for analyzing  
644 magnetotactic behavior. *Front. Microbiol.* 9, 1569. <https://doi.org/10.3389/fmicb.2018.01569>.

645 Cobb, R.E., Wang, Y., Zhao, H., 2015. High-efficiency multiplex genome editing of *Streptomyces*  
646 species using an engineered CRISPR/Cas system. *ACS Synth. Biol.* 4, 723-8.  
647 <https://doi.org/10.1021/sb500351f>.

648 Cox, B.L., Popa, R., Bazylnski, D.A., Lanoil, B., Douglas, S., Belz, A., Engler, D.L., Nealson, K.H.,  
649 2002. Organization and elemental analysis of P-, S-, and Fe-rich inclusions in a population of  
650 freshwater magnetococci. *Geomicrobiol. J.* 19, 387-406.  
651 <https://doi.org/10.1080/01490450290098504>

652 Frankel, R.B., Blakemore, R.P., Torres De Araujo, F.F., Esquivel, D.M.S., Danon, J., 1981.  
653 Magnetotactic bacteria at the geomagnetic equator. *Science* 212, 1269-70.  
654 <https://doi.org/10.1126/science.212.4500.1269>.

655 Goff, J., Yee, N., 2017. Tellurate enters *Escherichia coli* K-12 cells via the SulT-type sulfate transporter  
656 CysPUWA. *FEMS Microbiol. Lett.* 364. <https://doi.org/10.1093/femsle/fnx241>.

657 Grant, C.R., Amor, M., Trujillo, H.A., Krishnapura, S., Iavarone, A.T., Komeili, A., 2022. Distinct gene  
658 clusters drive formation of ferrosome organelles in bacteria. *Nature* 606, 160-164.  
659 <https://doi.org/10.1038/s41586-022-04741-x>.

660 Guo, F.F., Yang, W., Jiang, W., Geng, S., Peng, T., Li, J.L., 2012. Magnetosomes eliminate intracellular  
661 reactive oxygen species in *Magnetospirillum gryphiswaldense* MSR-1. *Environ. Microbiol.* 14,  
662 1722-9. <https://doi.org/10.1111/j.1462-2920.2012.02707.x>.

663 He, Y.Y., Hader, D.P., 2002. Involvement of reactive oxygen species in the UV-B damage to the  
664 cyanobacterium *Anabaena* sp. *J. photochem. Photobiol. B.* 66, 73-80. [https://doi.org/](https://doi.org/10.1016/s1011-1344(01)00278-0)  
665 [10.1016/s1011-1344\(01\)00278-0](https://doi.org/10.1016/s1011-1344(01)00278-0).

666 Hernandez, M.E., Newman, D.K., 2001. Extracellular electron transfer. *Cell Mol. Life Sci.* 58,  
667 1562-1571. <https://doi.org/10.1007/pl00000796>.

668 Jadhav, M., Prabhu, A., 2022. Metallic and polymeric green nanoplatfoms in oncology. *J. Appl.*  
669 *Microbiol.* 134, lxac044. <https://doi.org/10.1093/jambio/lxac044>.

670 Ji, W.J., Huang, H.M., Deng, A.H., Pan, C.Y., 2009. Effects of static magnetic fields on *Escherichia*  
671 *coli*. *Micron* 40, 894-898. <https://doi.org/10.1016/j.micron.2009.05.010>.

672 Jiang, W., Zhao, D.H., Li, Y., Tian, J.S., Wang, Z.F., Li, J.L., 2002. Submerged culture of  
673 *Magnetospirillum gryphiswaldense* under N-2-fixing condition and regulation of activity of  
674 nitrogen fixation. *Chin. Sci. Bull.* 47, 2095-2099. <https://doi.org/10.1360/02tb9455>.

675 Kolinko, I., Lohsse, A., Borg, S., Raschdorf, O., Jogler, C., Tu, Q., Posfai, M., Tompa, E., Plitzko, J.M.,  
676 Brachmann, A., Wanner, G., Muller, R., Zhang, Y.M., Schüler, D., 2014. Biosynthesis of  
677 magnetic nanostructures in a foreign organism by transfer of bacterial magnetosome gene  
678 clusters. *Nat. Nanotechnol.* 9, 193-197. <https://doi.org/10.1038/nnano.2014.13>.

679 Komelli, A., 2007. Molecular mechanisms of magnetosome formation *Annu Rev Biochem. Annual*  
680 *Review of Biochemistry*, vol 76. Annual Reviews, Palo Alto, pp 351-366.

681 Leila, H-G.J., Abolhassani, M., Hosseini, S.N., Ghareyazie, B., Ma'mani, L., Doroud, D., Behrouzi, A.,  
682 Ghorbani, M., 2019. Effects of electromagnetic fields exposure on the production of nanosized  
683 magnetosome, elimination of free radicals and antioxidant defense Systems in  
684 *Magnetospirillum gryphiswaldense* MSR-1. *J. Nano. Res.* 58, 20-31.  
685 <https://doi.org/10.4028/www.scientific.net/JNanoR.58.20>.

686 Letuta, U.G., Avdeeva, E.I., Berdinsky, V.L., 2014. Magnetic field effects in bacteria *E. coli* in the  
687 presence of Mg isotopes. *Russ. Chem. B.* 63, 1102-1106.  
688 <https://doi.org/10.1007/s11172-014-0555-1>.

689 Li, G.X., Bao, P., 2021. Transcriptomics analysis of the metabolic mechanisms of iron reduction  
690 induced by sulfate reduction mediated by sulfate-reducing bacteria. *FEMS Microbiol. Ecol.* 97.  
691 <https://doi.org/10.1093/femsec/fiab005>,

692 Li, H.D., Xie, R.N., Xu, X., Liao, X.R., Guo, J.X., Fang, Y.W., Fang, Z., Huang, J., 2022a. Static  
693 magnetic field inhibits growth of *Escherichia coli* colonies via restriction of carbon  
694 source utilization. *Cells* 11. <https://doi.org/10.3390/cells11050827>.

695 Li, J.H., Liu, P.Y., Menguy, N., Benzerara, K., Bai, J., Zhao, X., Leroy, E., Zhang, C.Q., Zhang, H., Liu,  
696 J.W., Zhang, R.R., Zhu, K.K., Roberts, A.P., Pan, Y.X., 2022b. Identification of  
697 sulfate-reducing magnetotactic bacteria via a group-specific 16S rDNA primer and correlative  
698 fluorescence and electron microscopy: Strategy for culture-independent study. *Environ.*  
699 *Microbiol.* 24, 5019-5038. <https://doi.org/10.1111/1462-2920.16109>.

700 Li, J.H., Liu, P.Y., Menguy, N., Zhang, X.L., Wang, J., Benzerara, K., Feng, L.J., Sun, L., Zheng, Y.,  
701 Meng, F.Q., Gu, L., Leroy, E., Hao, J.L., Chu, X., Pan, Y.X., 2022c. Intracellular silicification  
702 by early-branching magnetotactic bacteria. *Sci. Adv.* 8, eabn6045.  
703 <https://doi.org/10.1126/sciadv.abn6045>.

704 Li, J.H., Liu, P.Y., Tamaxia, A., Zhang, H., Liu, Y., Wang, J., Menguy, N., Zhao, X., Roberts, A.P., Pan,

705 Y.X., 2021a. Diverse intracellular inclusion types within magnetotactic bacteria: implications  
706 for biogeochemical cycling in aquatic environments. *J. Geophys. Res-Biogeosci.* 126.  
707 <https://doi.org/10.1029/2021jg006310>

708 Li, J.H., Pan, Y.X., Liu, Q.S., Qin, H.F., Deng, C.L., Che, R.C., Yang, X.A., 2010. A comparative study  
709 of magnetic properties between whole cells and isolated magnetosomes of *Magnetospirillum*  
710 *magneticum* AMB-1. *Chin. Sci. Bull.* 55, 38-44. <https://doi.org/10.1007/s11434-009-0333-x>.

711 Li, K.F., Wang, P.P., Chen, C.F., Chen, C.Y., Li, L.L., Song, T., 2017. Light irradiation helps  
712 magnetotactic bacteria eliminate intracellular reactive oxygen species. *Environ. Microbiol.* 19,  
713 3638-3648. <https://doi.org/10.1111/1462-2920.13864>.

714 Li, Y.J., 2021b. Redox control of magnetosome biomineralization. *J. Oceanol. Limno.* 39, 2070-2081.  
715 <https://doi.org/10.1007/s00343-021-0422-5>.

716 Li, Y.J., Katzmann, E., Borg, S., Schüler, D., 2012. The periplasmic nitrate reductase nap is required for  
717 anaerobic growth and involved in redox control of magnetite biomineralization in  
718 *Magnetospirillum gryphiswaldense*. *J. Bacteriol.* 194, 4847-4856.  
719 <https://doi.org/10.1128/jb.00903-12>.

720 Lin, W., Kirschvink, J.L., Paterson, G.A., Bazylinski, D.A., Pan, Y.X., 2019. On the origin of microbial  
721 magnetoreception. *Nat. Sci. Rev.* 7, 472-479. <https://doi.org/10.1093/nsr/nwz065>.

722 Lin, W., Zhang, W.S., Zhao, X., Roberts, A.P., Paterson, G.A., Bazylinski, D.A., Pan, Y.X., 2018.  
723 Genomic expansion of magnetotactic bacteria reveals an early common origin of magnetotaxis  
724 with lineage-specific evolution. *Isme J.* 12, 1508-1519.  
725 <https://doi.org/10.1038/s41396-018-0098-9>.

726 Liu, P.Y., Liu, Y., Ren, X., Zhang, Z., Zhao, X., Roberts, A.P., Pan, Y.X., Li, J.H., 2021. A novel  
727 magnetotactic alphaproteobacterium producing intracellular magnetite and calcium-bearing  
728 minerals. *Appl. Environ. Microbiol.* 87. <https://doi.org/10.1128/aem.01556-21>.

729 Lowe, S.E., Jain, M.K., Zeikus, J.G., 1993. Biology, ecology, and biotechnological applications of  
730 anaerobic bacteria adapted to environmental stresses in temperature, pH, salinity, or substrates.  
731 *Microbiol. Rev.* 57, 451-509. <https://doi.org/10.1128/membr.57.2.451-509.1993>.

732 Madsen, E.L., 2011. Microorganisms and their roles in fundamental biogeochemical cycles. *Curr. Opin.*  
733 *Biotechnol.* 22, 456-464. <https://doi.org/10.1016/j.copbio.2011.01.008>.

734 Moskowitz, B., Egli, R., 2005. Magnetic properties of magnetosomes in cultured magnetotactic

735 bacteria and in sediments: relationships with the environment. American Geophysical Union,  
736 Fall Meeting 2005:abstract #B24A-06.

737 Moskowitz, B.M., 1993. High-temperature magnetostriction of magnetite and titanomagnetites. J.  
738 Geophys. Res-Sol EA. 98, 359-371. [https://doi.org/ 10.1029/92JB01846](https://doi.org/10.1029/92JB01846).

739 Murat, D., Falahati, V., Bertinetti, L., Csencsits, R., Kornig, A., Downing, K., Faivre, D., Komeili, A.,  
740 2012. The magnetosome membrane protein, MmsF, is a major regulator of magnetite  
741 biomineralization in *Magnetospirillum magneticum* AMB-1. Mol. Microbiol. 85, 684-99.  
742 <https://doi.org/10.1111/j.1365-2958.2012.08132.x>.

743 Pan, W.D., Chen, C.F., Wang, X.K., Ma, Q.F., Jiang, W., Lv, J., Wu, L-F., Song, T., 2010. Effects of  
744 pulsed magnetic field on the formation of magnetosomes in the *Magnetospirillum* sp Strain  
745 AMB-1. Bioelectromagnetics 31, 246-251. <https://doi.org/10.1002/bem.20549>.

746 Pan, Y.X., Petersen, N., Winklhofer, M., Davila, A.F., Liu, Q.S., Frederichs, T., Hanzlik, M., Zhu, R.X.,  
747 2005. Rock magnetic properties of uncultured magnetotactic bacteria. Earth Planet Sci. Lett.  
748 237, 311-325. <https://doi.org/10.1016/j.epsl.2005.06.029>.

749 Philippe, N., Wu, L-F., 2010. An MCP-like protein interacts with the MamK cytoskeleton and is  
750 involved in magnetotaxis in *Magnetospirillum magneticum* AMB-1. J. Mol. Biol. 400,  
751 309-322. <https://doi.org/10.1016/j.jmb.2010.05.011>.

752 Rajalakshmi, A., Ramesh, M., Divya, E., Kavitha, K., Puvanakrishnan, R., Ramesh, B., 2022.  
753 Production and characterization of naturally occurring antibacterial magnetite nanoparticles  
754 from magnetotactic *Bacillus* sp. MTB17. J. Appl. Microbiol. 132,2683-2693.  
755 <https://doi.org/10.1111/jam.15395>.

756

757 Raschdorf, O., Forstner, Y., Kolinko, I., Uebe, R., Pitzko, J.M., Schüler, D., 2016. Genetic and  
758 ultrastructural analysis reveals the key players and initial steps of bacterial magnetosome  
759 membrane biogenesis. Plos Genetics 12. <https://doi.org/10.1371/journal.pgen.1006101>.

760 Roche, B., Aussel, L., Ezraty, B., Mandin, P., Py, B., Barras, F., 2013. Iron/sulfur proteins biogenesis in  
761 prokaryotes: Formation, regulation and diversity. Biochim. Biophys. Acta. 1827, 455-469.  
762 <https://doi.org/10.1016/j.bbabi.2012.12.010>.

763 Sanyal, S.K., Shuster, J., Reith, F., 2019. Cycling of biogenic elements drives biogeochemical gold  
764 cycling. Earth-Sci. Rev. 190, 131-147. <https://doi.org/10.1016/j.earscirev.2018.12.010>.

765 Schüler, D., 2002. The biomineralization of magnetosomes in *Magnetospirillum gryphiswaldense*. Int.  
766 Microbiol. 5:209-214. <https://doi.org/10.1007/s10123-002-0086-8>.

767 Schüler, D., 2007. Magnetoreception and magnetosomes in bacteria, vol 3. Springer.

768 Song, Z., Niu, C., Wu, H., Wei, J.P., Zhang, Y.X., Yue, T., 2019. Transcriptomic analysis of the  
769 molecular mechanisms underlying the antibacterial activity of IONPs@pDA-Nisin  
770 composites toward *Alicyclobacillus acidoterrestris*. ACS Appl. Mater. Interfaces 11,  
771 21874-21886. <https://doi.org/10.1021/acsami.9b02990>.

772 Spring, S., Bazylinski, D.A., 2002. Magnetotactic bacteria. The Prokaryotes:1-20.

773 Taherkhani, S., Mohammadi, M., Daoud, J., Martel, S., Tabrizian, M., 2014. Covalent binding of  
774 nanoliposomes to the surface of magnetotactic bacteria for the synthesis of self-propelled  
775 therapeutic agents. ACS Nano 8, 5049-5060. <https://doi.org/10.1021/nn5011304>.

776 Uebe, R., Schüler, D., 2016. Magnetosome biogenesis in magnetotactic bacteria. Nat. Rev. Microbiol.  
777 14, 621-637. <https://doi.org/10.1038/nrmicro.2016.99>.

778 Wan, J., Monteil, C.L., Taoka, A., Ernie, G., Park, K., Amor, M., Taylor-Cornejo, E., Lefevre, C.T.,  
779 Komeili, A., 2022. McaA and McaB control the dynamic positioning of a bacterial magnetic  
780 organelle. Nat. Commun. 13. <https://doi.org/10.1038/s41467-022-32914-9>

781 Wang, K., Ge, X., Bo, T., Chen, Q., Chen, G.J., Liu, W.F., 2011. Interruption of the denitrification  
782 pathway influences cell growth and magnetosome formation in *Magnetospirillum magneticum*  
783 AMB-1. Lett. Appl. Microbiol. 53, 55-62. <https://doi.org/10.1111/j.1472-765X.2011.03063.x>.

784 Wang, N., Qian, Z.X., Luo, M.W., Fan, S.J., Zhang, X.J., Zhang, L.Y., 2018. Identification of salt stress  
785 responding genes using transcriptome analysis in green alga *Chlamydomonas reinhardtii*. Int  
786 J. Mol. Sci. 19. <https://doi.org/10.3390/ijms19113359>.

787 Wang, P.P., Chen, C.Y., Wang, Q.M., Chen, H.T., Chen, C.F., Xu, J.S., Wang, X., Song, T., 2022. Tumor  
788 inhibition via magneto-mechanical oscillation by magnetotactic bacteria under a swing MF. J.  
789 Control. Release. 351, 941-953. <https://doi.org/10.1016/j.jconrel.2022.09.059>.

790 Wang, X.K., Ma, Q.F., Jiang, W., Lv, J., Pan, W.D., Song, T., Wu, L-F., 2008. Effects of hypomagnetic  
791 field on magnetosome formation of *Magnetospirillum magneticum* AMB-1. Geomicrobiol. J.  
792 25, 296-303. <https://doi.org/10.1080/01490450802258295>.

793 Wolf, M.W., Rizzolo, K., Elliott, S.J., Lehnert, N., 2018. Resonance raman, electron paramagnetic  
794 resonance, and magnetic circular dichroism spectroscopic investigation of diheme

795 cytochrome c peroxidases from *Nitrosomonas europaea* and *Shewanella oneidensis*.  
796 *Biochemistry* 57, 6416-6433. <https://doi.org/10.1021/acs.biochem.8b00732>.

797 Xie, C., Mao, X., Huang, J., Ding, Y., Wu, J., Dong, S., Kong, L., Gao, G., Li, C.Y., Wei, L., 2011.  
798 KOBAS 2.0: a web server for annotation and identification of enriched pathways and diseases.  
799 *Nucleic Acids Res.* 39, W316-22. <https://doi.org/10.1093/nar/gkr483>.

800 Yang, C.D., Takeyama, H., Tanaka, T., Hasegawa, A., Matsunaga, T., 2001. Synthesis of bacterial  
801 magnetic particles during cell cycle of *Magnetospirillum magneticum* AMB-1. *Appl. Biochem.*  
802 *Biotechnol.* 91, 155-160. <https://doi.org/10.1385/abab:91-93:1-9:155>.

803 Zhang, S.D., Petersen, N., Zhang, W.J., Cargou, S., Ruan, J., Murat, D., Santini, C.L., Song, T., Kato, T.,  
804 Notareschi, P., 2014. Swimming behaviour and magnetotaxis function of the marine bacterium  
805 strain MO-1. *Environ. Microbiol. Rep.* 6, 14-20. <https://doi.org/10.1111/1758-2229.12102>.

806 Zhang, W.J., Chen, C., Li, Y., Song, T., Wu, L-F., 2010. Configuration of redox gradient determines  
807 magnetotactic polarity of the marine bacteria MO-1. *Environ. Microbiol. Rep.* 2, 646-650.  
808 <https://doi.org/10.1111/j.1758-2229.2010.00150.x>.

809 Zhao, L.Z., Wu, D., Wu, L-F., Song, T., 2007. A simple and accurate method for quantification of  
810 magnetosomes in magnetotactic bacteria by common spectrophotometer. *J. Biochem. Biophys.*  
811 *Methods* 70, 377-383. <https://doi.org/10.1016/j.jbbm.2006.08.010>.